International Journal of Microwave and Wireless Technologies, 2012, 4(1), 81–91. © Cambridge University Press and the European Microwave Association, 2012
doi:10.1017/S1759078711001085

RESEARCH PAPER

Analysis of RF power amplifiers in LINC systems

RONALD MONTESINOS[1,2], CORINNE BERLAND[1,2], MAZEN ABI HUSSEIN[1,2], OLIVIER VENARD[1,3] AND PHILIPPE DESCAMPS[1]

LInear amplification using Non-linear Components (LINC) is an architecture that achieves linear power amplification for radio-frequency (RF) transmitters. This paper describes the impact of RF power amplifiers (PAs) class on the overall system performances. The linearity and efficiency of the LINC transmitter with different PA classes (AB, B, C, D, E, F, F^{-1}, and J) are evaluated and compared, in terms of error vector magnitude (EVM), adjacent channel leakage ratio (ACLR), and power added efficiency (PAE), for a 16QAM modulation having 5.6 dB peak to average power ratio. Simulations are performed using a gallium-nitride high electron mobility transistor (GaN HEMT) for a power amplifier with an output power of 10 W at 900 MHz.

Keywords: LINC transmitter, Power amplifiers, Chireix combiner, Load pull modulation, Power efficiency, linearity

Received 24 March 2011; Revised 8 November 2011; first published online 5 January 2012

I. INTRODUCTION

Modern wireless communication systems use digital modulation signals that must be transmitted linearly while preserving a high-power efficiency. Among all existing architectures, the LInear amplification using Non-linear Components (LINC) architecture is a promising solution for base station transmitters [1–3]. The key issue of this architecture is that the power amplifiers (PA) must be a perfect voltage source and the choice of the class of the PA is primordial to achieve this operation mode [4]. In this paper, we study the impact of some PA classes, namely, AB, B, C, D, E, F, and J, on both efficiency and linearity of the LINC transmitter. The comparative analysis of PAs is performed through extensive simulations using Agilent's advanced design system. The advantages and drawbacks of this architecture are then demonstrated. PAs are simulated using a gallium-nitride high electron mobility transistor (GaN HEMT) model from Cree to achieve an output power of 10 W at 900 MHz. Linearity and efficiency performances of the transmitter are evaluated in terms of error vector magnitude (EVM), adjacent channel leakage ratio (ACLR), power added efficiency (PAE), using a 16QAM modulation.

[1]LaMIPS, Laboratoire Commun NXP-CRISMAT UMR 6508 CNRS ENSICAEN UCBN, Caen, France
[2]Dép. Systèmes Electroniques, ESIEE Paris, Cité Descartes, BP99, 93162 Noisy-le-Grand, France
[3]Dép. Télécommunications, ESIEE Paris, Cité Descartes, BP99, 93162 Noisy-le-Grand, France
Corresponding author:
R. Montesinos
Email: r.montesinos@esiee.fr

This paper is organized as follows: Section II describes the operation principle of the LINC architecture. The combiners for signal recombination at the output are presented in Section III. The performances of the simulated radio-frequency (RF) PAs are presented in Section IV. In Section V, we elaborate on how the performance of LINC transmitters is heavily dependent on the class of the PAs used. A 16QAM modulated signal is used for this study. Finally, conclusions are given in Section VI.

II. LINC ARCHITECTURE

The principle of operation of the LINC transmitter is depicted in Fig. 1. The input signal $S_{in}(t)$, with variable envelope $r(t)$ and phase $\varphi(t)$, is separated into two constant envelope signals, $S_1(t)$ and $S_2(t)$, by the signal component separator (SCS):

$$\begin{aligned} S_{in}(t) &= r(t)e^{j(wt+\varphi(t))} = r_{max}\cos\theta(t)e^{j(wt+\varphi(t))} \\ &= \frac{r_{max}}{2}(e^{j\theta(t)} + e^{-j\theta(t)})e^{j(wt+\varphi(t))} \\ &= S_1(t) + S_2(t), \end{aligned} \quad (1)$$

where

$$S_1(t) = \frac{r_{max}}{2}e^{j(wt+\varphi(t)+\theta(t))}, \quad (2)$$

$$S_2(t) = \frac{r_{max}}{2}e^{j(wt+\varphi(t)-\theta(t))} \quad (3)$$

https://doi.org/10.1017/S1759078711001085 Published online by Cambridge University Press

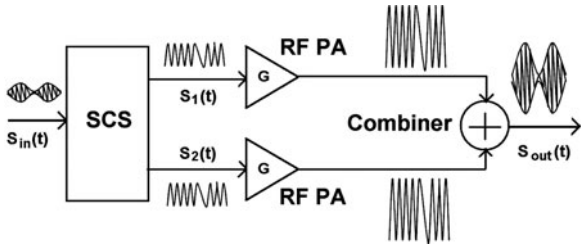


Fig. 1. LINC system topology.

with r_{max} the maximum value of $r(t)$ and $\theta(t)$ equal to

$$\theta(t) = \arccos\left(\frac{r(t)}{r_{max}}\right). \tag{4}$$

The principle of signal decomposition is illustrated in Fig. 2 using a vectorial representation.

Signals $S_1(t)$ and $S_2(t)$ are amplified with two power efficient PAs with a power gain G. Envelope amplitude variation is restored at the output of the combiner by the simple addition of the two amplified signals. The output signal is then given by

$$S_{out}(t) = G(S_1(t) + S_2(t)) = GS_{in}(t). \tag{5}$$

III. SIGNAL RECOMBINATION

The restoration of the original signal waveform at the output of the LINC transmitter is realized by an RF combiner. In the literature, we can find two types of combiners: Wilkinson combiner which is matched and *lossy* and Chireix combiner which is unmatched and *lossless* [5]. Combiner efficiency, denoted η_{comb}, is defined in equation (6) as the ratio of the active power P_{out} delivered to the output load to the sum of the apparent power in the input of each line P_{app1} and P_{app2} [2, 6]:

$$\eta_{comb} = \frac{P_{out}}{P_{app1} + P_{app2}}. \tag{6}$$

A) Wilkinson combiner

The topology of this combiner is given in Fig. 3. Z_c is the characteristic impedance of the two quarter-wavelength transmission lines, R_S represents the impedance seen at each input of the combiner, and R_L is the output load of the combiner.

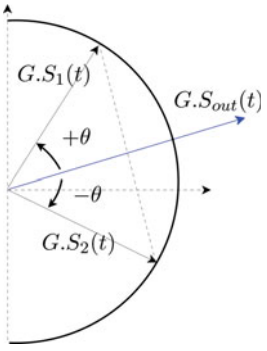


Fig. 2. LINC vectorial representation.

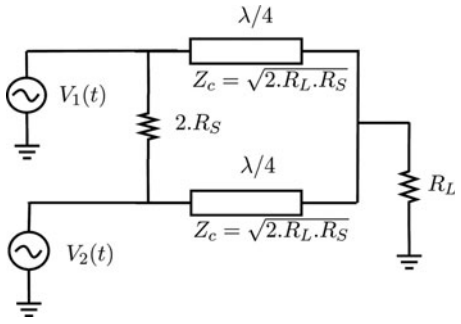


Fig. 3. Wilkinson combiner.

The two outphased input signals denoted $V_1(t)$ and $V_2(t)$ and having a constant amplitude V, can be written as

$$\begin{aligned} V_1(t) &= Ve^{j(wt+\theta(t))} = V_1e^{j(wt)}, \\ V_2(t) &= Ve^{j(wt-\theta(t))} = V_2e^{j(wt)}, \end{aligned} \tag{7}$$

where V_1 and V_2 are complex conjugates

$$\begin{aligned} V_1 &= V(\cos(\theta) + j\sin(\theta)), \\ V_2 &= V(\cos(\theta) - j\sin(\theta)), \end{aligned} \tag{8}$$

thus we can demonstrate that the Wilkinson efficiency, $\eta_{Wilkinson}$, can be expressed as a function of the outphasing angle $\theta(t)$ as follows [5]:

$$\eta_{wilkinson} = \cos^2(\theta). \tag{9}$$

The efficiency of this combiner is linked to the fact that the two PAs deliver a constant maximum power at both inputs of the combiner and the output power depends only on the envelope of the signal, that is to say $r(t)$ and thus the outphasing angle $\theta(t)$ as defined in equation (4).

B) Chireix combiner

The Chireix combiner is composed of two quarter-wavelength transmission lines having a characteristic impedance Z_c and connected to the output load of combiner R_L [6], as presented in Fig. 4.

Let us first make the analysis of this combiner (Fig. 4), without the inductor L and the capacitor C (non-compensated Chireix combiner). The output current I_o and output voltage

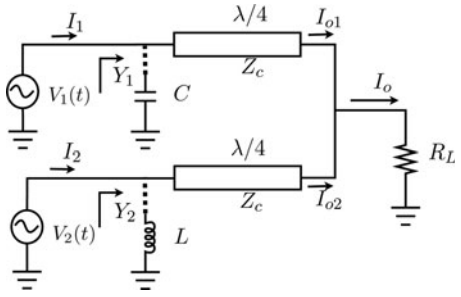


Fig. 4. Chireix combiner with compensation.

https://doi.org/10.1017/S1759078711001085 Published online by Cambridge University Press

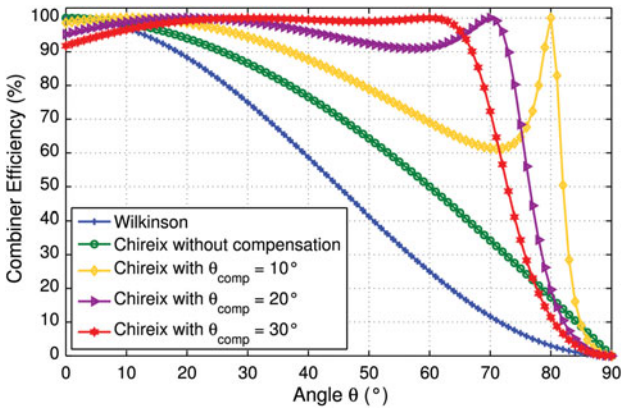


Fig. 5. Efficiency of Wilkinson combiner and Chireix combiner (with and without compensation)

V_o are given in equation (10) from general equations of transmission lines, where I_{o1} and I_{o2} are the two output currents:

$$I_o = I_{o1} + I_{o2} = \frac{2V\cos\theta}{jZ_c},$$
$$V_o = I_o R_L = \frac{2V\cos\theta}{jZ_c} R_L. \tag{10}$$

The input currents are

$$I_1 = I_2 = \frac{jV_o}{Z_c} = \frac{2VR_L\cos(\theta)}{Z_c^2}. \tag{11}$$

Thus, the admittances Y_1 and Y_2, seen by each PA, are complex conjugate:

$$Y_1 = \frac{I_1}{V_1} = G_o - jB_o,$$
$$Y_2 = \frac{I_2}{V_2} = G_o + jB_o = Y_1^* \tag{12}$$

with G_o and B_o

$$G_o = \frac{2R_L\cos^2(\theta)}{Z_c^2},$$
$$B_o = \frac{R_L\sin(2\theta)}{Z_c^2}. \tag{13}$$

In order to increase the combiner efficiency, susceptance B_o should be compensated for, at a chosen angle θ_{comp}, by introducing a parallel admittance calculated from equation (13) using either stubs or passive elements, e.g. C and L with dotted lines in Fig. 4 and with the values

$$C = \frac{B_o}{\omega} = \frac{R_L\sin(2\theta_{comp})}{2\pi f Z_c^2},$$
$$L = \frac{1}{\omega B_o} = \frac{Z_c^2}{2\pi f R_L\sin(2\theta_{comp})}. \tag{14}$$

Equations (10)–(13) are calculated taking into account only the two sources, both transmission lines and the output load R_L in the Fig. 4. From equation (14) and for the following equations, values of L and C will be considered, i.e. the compensation represented by θ_{comp}, unless stated otherwise.

According to the PA class and the compromise between power efficiency and linearity of the overall transmitter, this compensation angle has to be chosen carefully [5, 7].

The efficiency of the Chireix combiner is defined as

$$\eta_{Chireix} = \frac{|V_o||I_o|}{|V_1|^2|Y_1| + |V_2|^2|Y_2|} \tag{15}$$

and is expressed in function of θ, without and with compensation, as follows:

$$\eta_{CH\ without\ comp} = \cos(\theta), \tag{16}$$

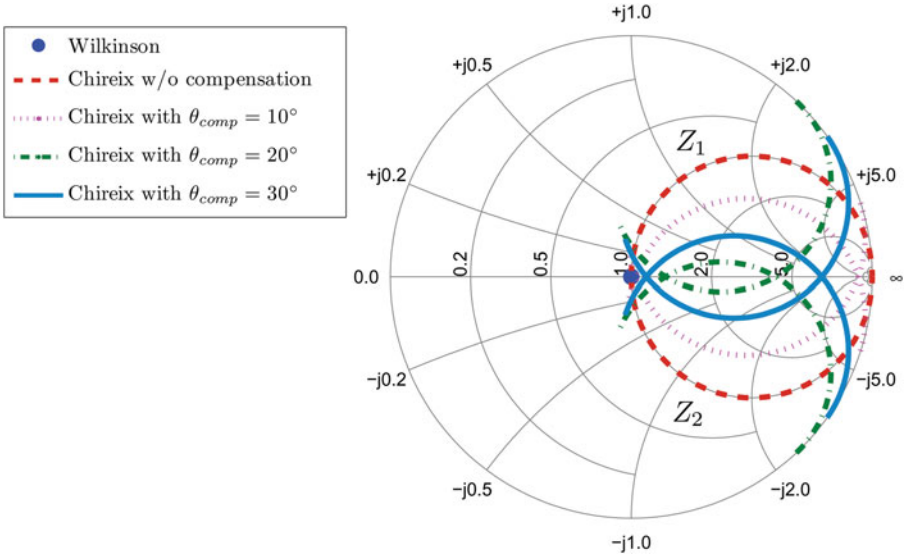


Fig. 6. Smith chart for different impedances with Wilkinson and Chireix combiner (with and without compensation). Z_1 and Z_2 represent, respectively, the impedances at the upper and lower branches (θ (0–90°)).

https://doi.org/10.1017/S1759078711001085 Published online by Cambridge University Press

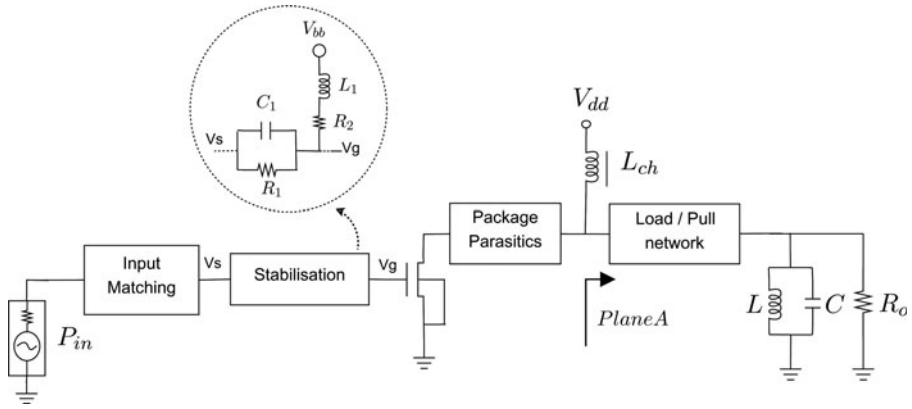


Fig. 7. Topology for class AB, B, C, and J PAs.

$$\eta_{CH\ with\ comp} = \frac{2\cos^2(\theta)}{\sqrt{2\cos^2(\theta)^2 + \sin(2\theta) - \sin(2\theta_{comp})^2}}. \quad (17)$$

Figure 5 shows both combiners efficiency calculated from equations (9), (16), and (17). For the Chireix combiner, efficiency is evaluated without and with compensation for different values of θ_{comp}: 10°, 20°, and 30°.

These results demontrate that the Chireix combiner has a higher efficiency than the Wilkinson combiner. Nevertheless, the Chireix non-isolating behavior modifies its input impedances according to the angle θ from equation (4) and thus the power transmitted by each PA. This highlights the need for performance analysis of the LINC architecture using a Chireix combiner with different PA classes. A LINC transmitter with saturated class B PAs using a Chireix combiner can be founded in [8]. An analysis using class AB and class F PAs for this architecture is shown in [9].

In addition, the impedances Z_1 and Z_2 seen by each PA are determined from equation (12) as follows:

$$\begin{aligned} Z_1 &= \frac{1}{Y_1} = \frac{Z_c^2}{2R_L}(1 + j\mathrm{tg}(\theta)), \\ Z_2 &= \frac{1}{Y_2} = \frac{Z_c^2}{2R_L}(1 - j\mathrm{tg}(\theta)). \end{aligned} \quad (18)$$

Figure 6 represents these impedances for each combiner, Wilkinson and Chireix (without and with compensation), as a function of the angle θ in the Smith chart. Since Wilkinson combiner is isolated, Wilkinson combiner impedances are placed at the center of the Smith chart, whereas,

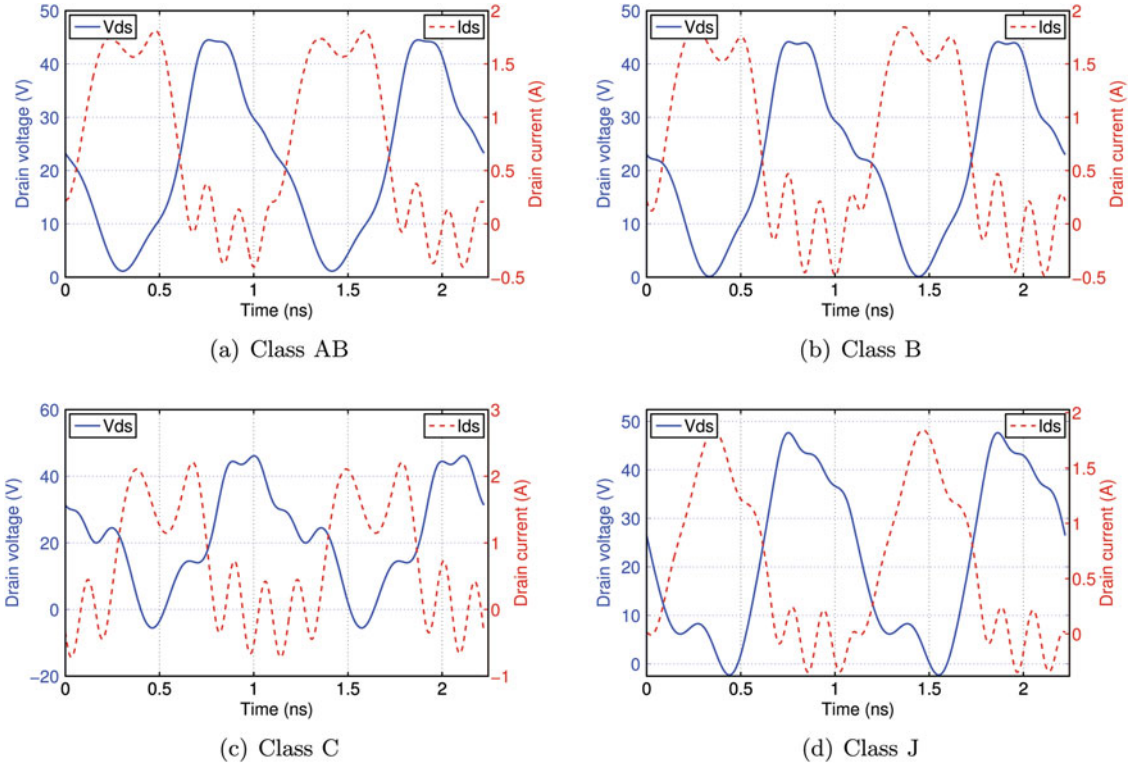


Fig. 8. V_{ds} and I_{ds} curves simulated for classes AB, B, C, and J PAs.

https://doi.org/10.1017/S1759078711001085 Published online by Cambridge University Press

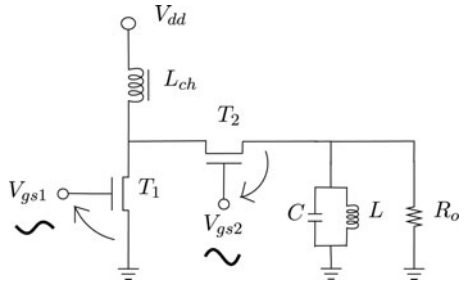


Fig. 9. CMCD power amplifier with parallel-resonant circuit [14].

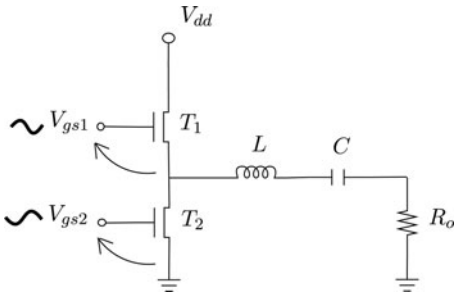


Fig. 10. VMCD power amplifier with a series-resonant circuit [14].

the input impedances at the input of Chireix combiner are angle dependent, as shown in Fig. 6. As a result, the compensation in Chireix combiner has an important impact on the linearity of the whole system as it modifies the PAs transmitted power. In order to achieve the best transfer of power and avoid the power loss between the PA and the combiner, output load of PAs need to be carefully matched with the impedances Z_1 and Z_2, at an appropriate value of θ_{comp}. Thus, these curves are very useful to analyze the behavior of load modulation of the PAs. Figure 6 is determined with the assumption that the output impedance of PA is 50Ω.

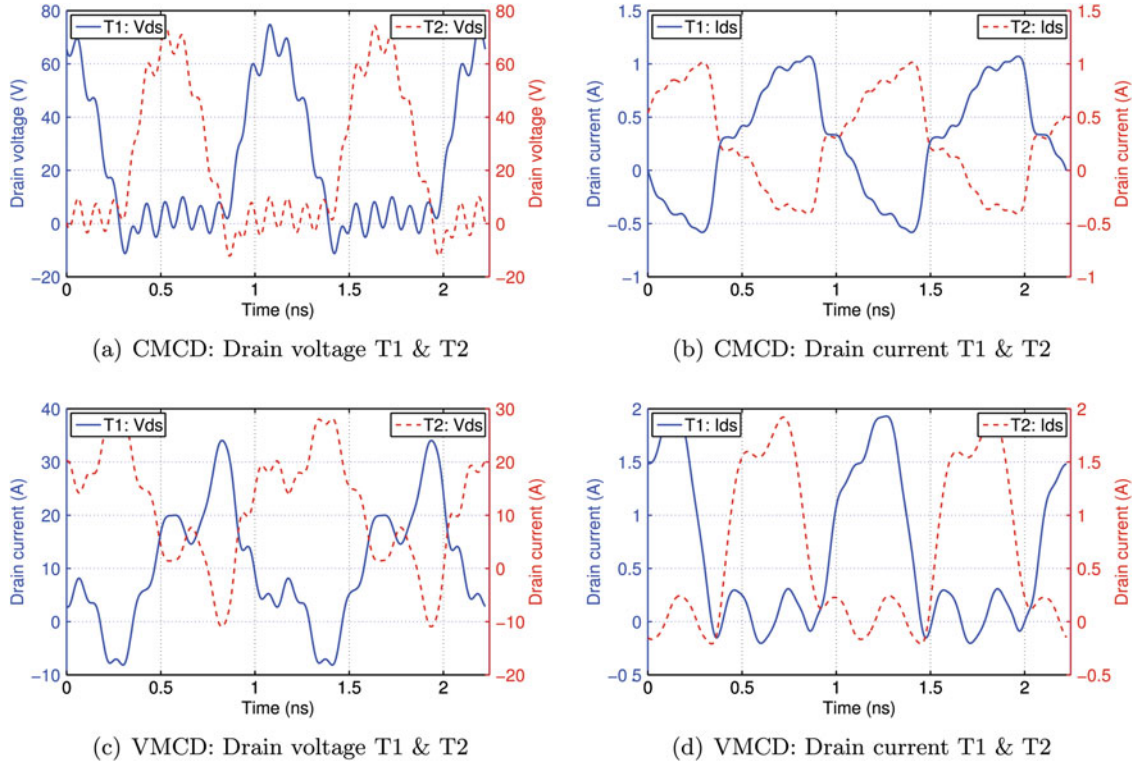
In the following section, we review the classes of RF PAs simulated for this study.

IV. RF POWER AMPLIFIERS

PAs are often classified according to their biasing and their operating classes [10]. A first classification relies on biasing classes PAs (classes A, AB, B, or C): the driving signal is a sinusoidal waveform and the active device behaves as a current source. Classes AB, B, and C PAs are chosen for our study. A second classification is related to the active device dynamic operating conditions and consequently to the matching network terminating conditions. In this case, basically two wide categories are identified, namely *current-mode* and *switching-mode* PAs. In the former case, referred, as classes F, F^{-1}, and J, the active device acts as voltage controlled or current controlled current source. Whereas, in the latter family, referred as classes D, E, G, and H, the active devices behave as switches. Class D PAs can operate either in current mode class D (CMCD) or in voltage mode class D (VMCD). For our study, in addition to the biasing classes AB, B, and C, we will consider PA classes from the second category namely CMCD, VMCD, E, F, F^{-1}, and J.

A) Design of classes RF PAs

The various PAs are designed using a 15 W GaN Cree transistor (CGH27015) to achieve an output power of 40 dBm (10W) at 900 MHz. Transistor model includes



(a) CMCD: Drain voltage T1 & T2

(b) CMCD: Drain current T1 & T2

(c) VMCD: Drain voltage T1 & T2

(d) VMCD: Drain current T1 & T2

Fig. 11. V_{ds} and I_{ds} curves simulated on both transistor for VMCD and CMCD.

https://doi.org/10.1017/S1759078711001085 Published online by Cambridge University Press

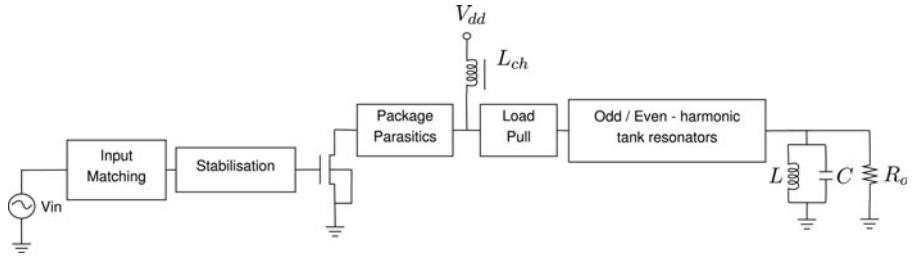


Fig. 12. Topology for class F (with odd harmonics) and F^{-1} (with even harmonics) PAs.

intrinsic and packaging parasitic components. This transistor model has a typical drain–source breakdown voltage of 140 V. All PAs are designed with 22 V supply voltage source. For this value of drain–source voltage (V_{ds}), the maximal drain current (I_{ds}) is equal to 2.9 A and the typical gate threshold voltage is equal to −3.3 V. The conduction angles for biasing classes PAs are determined in fonction of gate voltages.

The design of classes AB, B, and C PAs follows the guideline given in [11]. In order to attain the output power with a better efficiency, the conduction angle is set to $\alpha = 1.2\pi$ for the class AB PA and $\alpha = 0.85\pi$ for the class C PA. The design of the class J PA is based on the design of a class AB PA as explained in [11, 12]. The general topology for these PAs is depicted in Fig. 7 showing blocks of input matching, stabilization, and load pull network where the L-C network resonnates at the operating frequency. The transistor is unconditionally stable in wideband up to 10 GHz, thanks to the stabilization network [13]. By presenting optimal impedance with load pull network at plane A (Fig. 7) the maximal output power is transfered toward the output load R_o. This value should be seen by each branch in the input of the Chireix combiner. Input matching network is designed to achieve an input impedance of 50Ω. For classes AB, B, and C, the drain current is roughly half-sinusoidal and the drain voltage sinusoidal except for class J whose drain voltage is also half-sinusoidal [12] as shown in Fig. 8.

The design of operating classes PAs is based on the equations from [14, 15]. CMCD and VMCD PAs use two transistors in switched mode with outphased bias of gate–source voltage each one to other, see Figs. 9 and 10. In CMCD, drain current has a half-square wave while voltage is half-sine, whereas in VMCD, current is half-sinusoidal and voltage half-square, see Fig. 11.

The class E is a switched mode PA with a specific output network made of a shunt capacitor connected to the drain of the transistor (in our case in the output at plane A) and a series L-C resonator [15]. Drain current has a half-sinusoidal fraction shape and drain voltage is slightly half-sinusoidal [14, 15] as shown in Fig. 13(a).

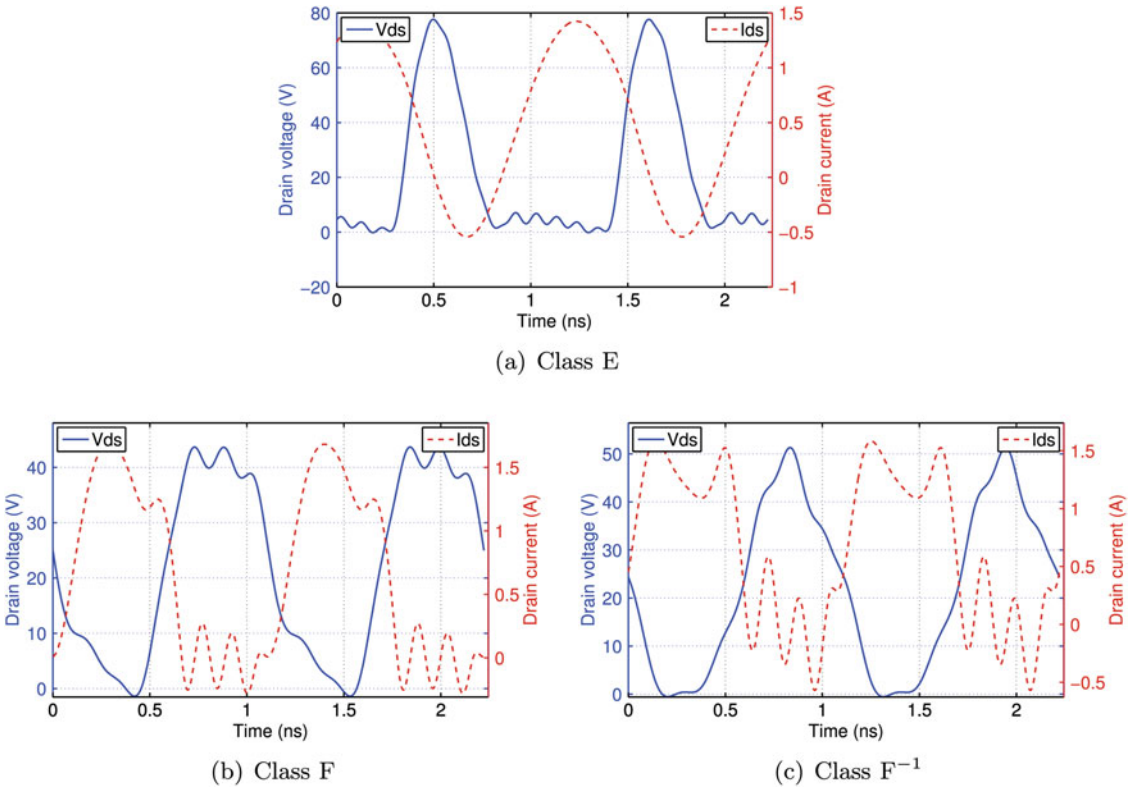


Fig. 13. Drain voltage and current for classes E, F, and F^{-1}.

https://doi.org/10.1017/S1759078711001085 Published online by Cambridge University Press

Table 1. Drain efficiency (DE) for the classes of RF PA designed.

Class	AB	B	C	CMCD	VMCD	E	F	F^{-1}	J
DE (%)	60	62	64	83	71	88	71	69	75

Classes F and F^{-1} PAs work with a biased transistor in class AB [16]. Shunt LC resonator circuits for odd (class F) or even (class F^{-1}) harmonics are added in series to increase the efficiency and to give a square waveform to the drain voltage and drain current, respectively [17, 16]. Topology for these classes is shown in Fig. 12 where each block, except for odd/even – harmonic tank resonators, behaves like in Fig. 7. Drain current in class F and drain voltage in class F^{-1} are half-sine, see Figs. 13(b) and 13(c). Harmonic manipulation approaches for second and third harmonic control for the design of these classes can also be considered (harmonic manipulated PA) [18, 19]. Harmonic tank resonators for class F and F^{-1} were designed up to fifth and fourth hamonics, respectively [14, 15].

B) Linearity and efficiency of the simulated PAs

Drain efficiency is computed for all classes of PAs. This efficiency is defined as the ratio between the active output power to DC power. The values obtained are shown in Table 1 and are slightly lower than theoretical values. PAs from operating classes exhibit the highest efficiency values, as expected.

Harmonic distortion (HD) is used to evaluate the linearity performance. HD is defined as the ratio between the power at the fundamental frequency and a given harmonic. Let us denote HD_2 and HD_3 for the second and the third harmonic distortion. The values obtained for all classes of PAs are shown in Table 2.

We notice that class E and CMCD power amplifiers have the best efficiency performance with 88 and 83% drain efficieny, respectively. Also classes F and F^{-1} have the best linearity performance for HD_2 and HD_3, respectively.

V. LINC TRANSMITTER PERFORMANCES

In this section we investigate the performances of the LINC transmitter designed with the previously presented PAs and the Chireix combiner. The circuit topology used for our simulations is depicted in Fig. 14. $S_1(t)$ and $S_2(t)$ represent two outphased power generators from equations (2) and (3). Vo_1 and Vo_2 represent the input voltages of the combiner at the upper and lower branches, respectively, and Vo is the output voltage. Values of C_{comp} and L_{comp} are taken from equation (14), Z_c and R_L are, respectively, the characteristic impedance of each quarter-wavelength transmission line and the output load of Chireix combiner. The analysis is conducted for two values of the compensation angle θ_{comp}: 10 and 30°.

A) Global performances of the LINC transmitter

First, we characterize the transmitter with sinusoidal input signals, $S_1(t)$ and $S_2(t)$ in Fig. 14, as a function of the outphasing angle $\theta(t)$, i.e. $S_1(t)$ and $S_2(t)$ with positive and negative values of θ, respectively.

The overall PAE is calculated to analyze the impact of each class on the efficiency. This PAE is defined as follows:

$$\eta_{PAE} = \frac{P_{out} - (P_1 + P_2)}{P_{DC}} \tag{19}$$

with P_{out} the active output power delivered to the load R_L, P_1, and P_2 the power at the input of the PAs and P_{DC} the sum of the DC power consumed by the two PAs.

The PAE is plotted in function of the outphasing angle θ for two values of θ_{comp}: Fig. 15(a) for $\theta_{comp} = 10°$, and Fig. 15(b) for $\theta_{comp} = 30°$.

Maximal PAE values are presented for each PA class in Table 3.

The maximum efficiency is obtained for the class E PA and for $\theta_{comp} = 30°$ its efficiency remains above 80% for an outphasing angle between 15 and 60°. Among biased PAs, the class J has the best efficiency performance with a maximum value of 69% and remains above 60% up to an outphasing angle value of 30°. However, according to Fig. 5, the compensation of the Chireix combiner should have maintained a good efficiency performance over a widest range of the outphasing angle. For non-switched mode PAs one may notice that the value of θ_{comp} has a lower impact than expected on this widening effect.

The linearity of the transmitter has been also studied with a 16QAM modulated signal. For this, we draw the equivalent AM/AM transfer function of the system, for each PA class, defined as the output power delivered to R_L versus the theoretical input power of PAs calculated from the ideal sum of the two voltage signals: $S_1(t)$ and $S_2(t)$. These transfer functions are plotted in Fig. 16 using a 16QAM modulation for the two compensation angles, $\theta_{comp} = 10$ and 30°. Thus, the impact of each class of PA on the linearity of the whole system is observed.

The analysis of these curves demonstrates that the compensation of the Chireix combiner modifies the linear behavior of the entire system: the lower compensation angle, the better the linearity. Only CMCD, class F^{-1} and class F PAs to a lesser extent, present an almost linear AM/AM slope close to unity. For the other classes, the AM/AM curves exhibit a distortion that is due to the unmatching effect of the combiner versus the outphasing angle, i.e. the load modulation effect. Indeed, the fact that the PAs do not have their optimum impedances at their outputs modifies both the amplitude and the

Table 2. HD for the classes of RF PA designed.

Class	AB	B	C	CMCD	VMCD	E	F	F^{-1}	J
HD_2 (dB)	32.3	31.2	33	42.5	48.3	30.2	40	72	31.2
HD_3 (dB)	40	40.4	34.7	44	38.2	45.2	60.5	44	44.2

https://doi.org/10.1017/S1759078711001085 Published online by Cambridge University Press

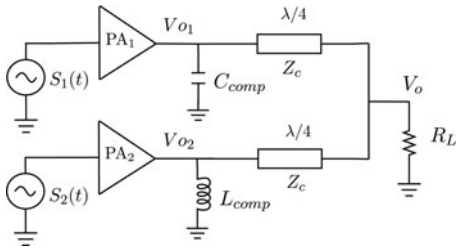


Fig. 14. LINC architecture: Chireix combiner with compensation components and RF PAs.

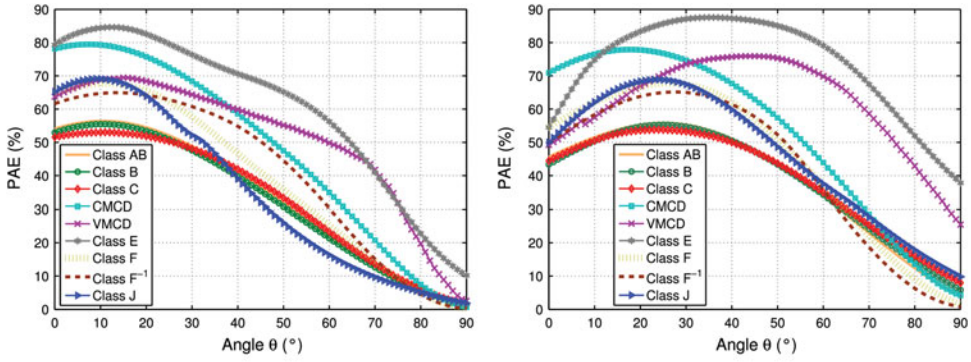
phase of the transmitted signals $S_1(t)$ and $S_2(t)$. This results in a real outphasing angle lower than expected and so in a higher output power. Only a phase predistortion before the PA can compensate for this compression of the output power dynamic range. According to the PA class, this phenomenon has more or less impact. Unfortunately, the class E PA which presents the best efficiency is highly affected by this problem.

AM/PM transfer functions for all PAs are depicted in Fig. 17 for each compensation angle. These curves represent the difference of phases between the output and input voltages versus the theoretical input power of PAs as calculated in Fig. 16. Only class F PA presents a quasi-linear AM/PM curve for almost all levels of input power with a phase variation less than 5°. CMCD and class B PAs present a linear behavior between 15 and 25dBm of input power, whereas class F^{-1} and class E PAs are the most affected with phase variations up to 40 and 30°, respectively. Although the phase variations for class F^{-1} is significant, it is interesting to note that this class offers an acceptable linearity as will be shown by the results of the next section.

The distortion observed with AM/AM curves and AM/PM curves are linked to the load modulation effect. This load modulation effect is illustrated in Fig. 18 where the two load impedances presented to the PAs by the Chireix combiner are plotted in function of the angle θ and for three PAs classes: E, F, and inverse F. Z_1 and Z_2 are, respectively, the load impedances in the upper and lower branches of the LINC transmitter. The main point to note is that the impedances are not anymore complex conjugate. This is linked to the fact that the power transmitted by each PA do not results in voltages (V_{O1} and V_{O2} in Fig. 14) with the same amplitude and opposite angles as theoretically expected, thus impacting on the value of these impedances. We already highlighted that class E was highly affected by the load effect on the AM/AM and AM/PM curves. Here we can notice that the input impedances of the Chireix combiner

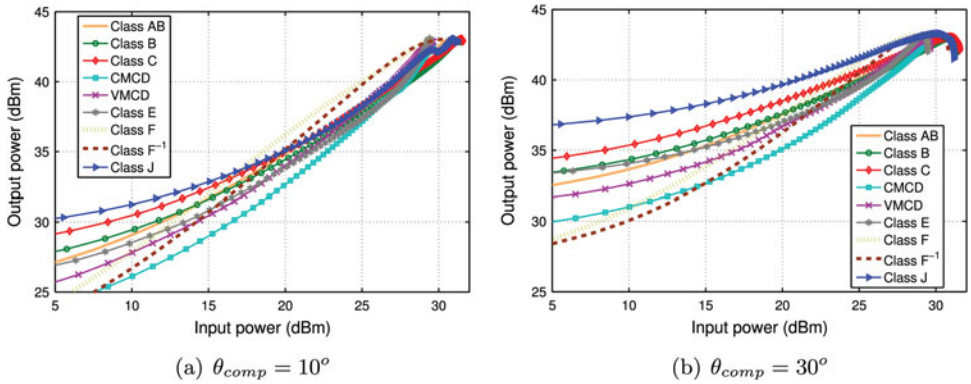
Table 3. Maximum PAE for the different PA classes studied.

Class	AB	B	C	CMCD	VMCD	E	F	F^{-1}	J
PAE % ($\theta_{comp} = 10^o$)	56	55	53	79	69	84	67	65	69
PAE % ($\theta_{comp} = 30^o$)	56	55	54	78	76	87	68	65	69



(a) $\theta_{comp} = 10^o$ (b) $\theta_{comp} = 30^o$

Fig. 15. PAE in LINC transmitter for each PA class.



(a) $\theta_{comp} = 10^o$ (b) $\theta_{comp} = 30^o$

Fig. 16. AM/AM transfer function for all PA classes with a 16QAM modulation.

https://doi.org/10.1017/S1759078711001085 Published online by Cambridge University Press

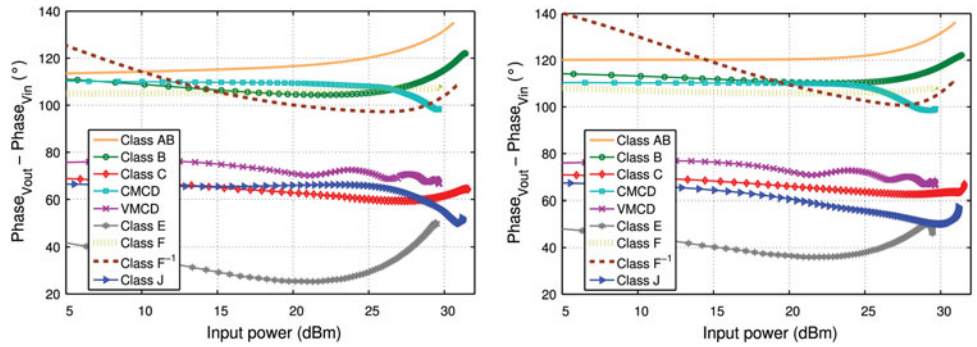


Fig. 17. AM/PM transfer function for all PA classes with a 16QAM modulation.

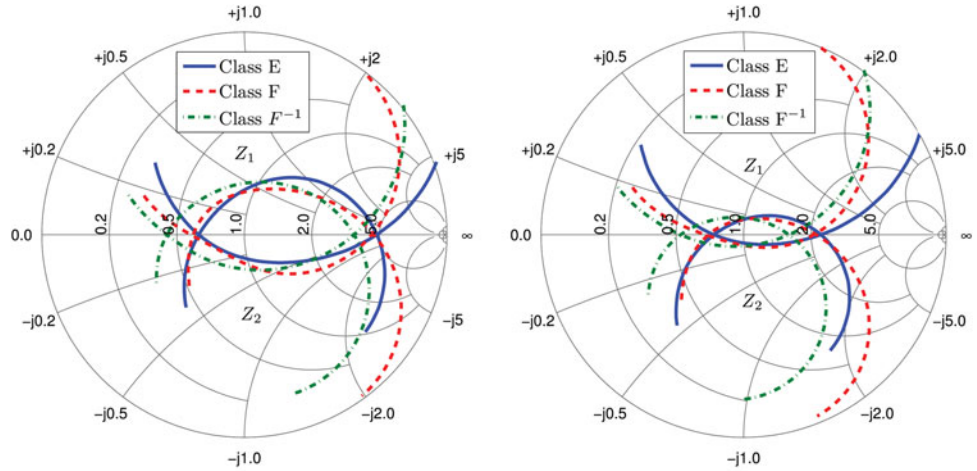


Fig. 18. Smith chart for classes E, F, and F^{-1} PAs. Z_1 and Z_2 represent, respectively, the impedances at the upper branch and lower branches (θ (0–90°)).

are, for the class E, not at all complex conjugate and even more completely different from the ideal impedances presented in Fig. 6. This effect is less visible for the inverse F PA, resulting in more linearity.

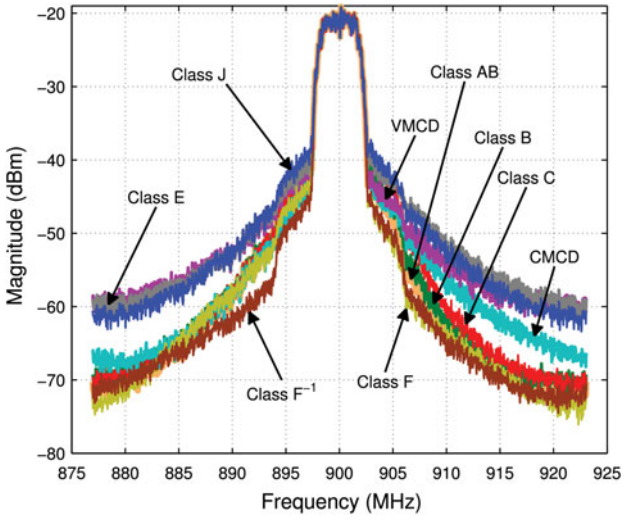


Fig. 19. Output spectrum of 16QAM modulation with all classes of PAs.

In the following section, we present the performances of the transmitter in terms of EVM, ACLR, and PAE using a 16QAM – modulated signal. These simulations are realized with $\theta_{comp} = 30^o$ that corresponds to the angle that gives the best efficiency.

B) Performances with a 16QAM – modulated signal

Simulations are carried out in this section using a 16QAM modulation with a 3.84 MHz symbol frequency and a roll – off equal to 0.35. As mentioned previously, the compensation angle used for the simulations presented here is set to 30°.

Figure 19 shows the spectrum at the output of the transmitter for all PA classes.

EVM and ACLR values are shown in Table 4. ACLR is calculated with ± 5 MHz offset for the lower (ACLR1) and upper (ACLR2) bands.

These results confirm the observations mentioned in the previous section: CMCD, class F and F^{-1} PAs give the best linearity performance with an EVM lower than 7% and ACLR values higher than 25 dB.

The average PAE is calculated for the 16QAM modulation, see Table 5. The mean power for this modulation corresponds to a mean outphasing angle of 60°: classes F and F^{-1} present

https://doi.org/10.1017/S1759078711001085 Published online by Cambridge University Press

Table 4. EVM and ACLR for a 16QAM modulation.

Class	AB	B	C	CMCD	VMCD	E	F	F^{-1}	J
EVM (%)	9.8	10.7	12	7	8.8	11.2	7	6	13.5
ACLR1 (dBc)	24.3	24	23.8	25.7	23	22	25.6	28	21
ACLR2 (dBc)	26	24.7	22.4	27.8	24.5	21.7	29.7	29	21

Table 5. Average PAE (%) of a 16QAM modulation in LINC transmitter with all PAs.

Class	AB	B	C	CMCD	VMCD	E	F	F^{-1}	J
PAE (%)	36.5	37.5	39.4	52	63.5	70.6	43	38.7	41.7

PAE values of the order of 40%. As predicted, the best efficiency for this modulation is obtained for the class E PA.

VI. CONCLUSIONS

In this paper, we present a detailed comparative analysis of the LINC transmitter performances with different PA classes. This helpful understanding is represented and studied by equations, circuits, and simulations. A Chireix combiner is used for signal recombination in order to achieve high efficiency. Input impedances variation, i.e. load pull effect, of this combiner is due to the non-isolating behavior at the output of the PAs and affects substantially the overall performance. In this work, we demonstrate that this impact is highly dependent on the class of the PAs used and the compensation angle of the combiner as well.

Better efficiencies are achieved for class E, VMCD PAs but to the detriment of linearity with EVM values higher than 9%. On the other hand, the best choice in terms of linearity is the class F^{-1} PA with an EVM below 6% and an average efficiency of about 40% for a 16QAM modulation. Other choices to achieve a good linearity can be class F and CMCD. CMCD and VMCD require two transistors for their implementation, whereas the other classes require only one transistor.

The compression of the output power dynamic range is the main drawback of the use of a Chireix combiner. A predistortion of the outphasing angle appears to be a promising technique to alleviate this weak point. Such predistortion approach could allow to implement highly linear and efficient LINC transmitter using a Chireix combiner.

Some perspectives and upcoming works of this study are the implementation on Printed Circuit Board (PCB) and test of classes of PAs corresponding to the best trade – off between efficiency and linearity.

ACKNOWLEDGEMENTS

This work is realized within an European Catrene Project: PANAMA. We would like to thank Cree for providing their GaN HEMT model.

REFERENCES

[1] Cox, D.: Linear amplification with nonlinear components. IEEE Trans. Commun., **12** (1974), 1942–1945.

[2] Raab, F.: Efficiency of outphasing RF power-amplifier systems. IEEE Trans. Commun., **12** (1985), 1094–1099.

[3] Raab, F. et al.: Power amplifiers and transmitters for RF and microwave. IEEE Trans. Microw. Theory Tech., **3** (2002), 814–826.

[4] Yao, J.; Long, S.: Power amplifier selection for LINC applications. IEEE Trans. Circuits Syst. II, **8** (2006), 763–767.

[5] Birafane, A.; El-Asmar, M.; Kouki, A.B.; Helaoui, M.; Ghannouchi, F.M.: Analyzing LINC systems. IEEE Microw. Mag., **5** (2010), 59–71.

[6] Chireix, H.: High power outphasing modulation. Proc. Inst. Radio Eng., **11** (1935), 1370–1392.

[7] Bi, J.: Chireix's LINC Power Amplifier for Base Station applications using GaN devices with load compensation, Master Thesis, TuDelft, 2008.

[8] Hakala, I. et al.: A 2.14-GHz Chireix outphasing transmitter. IEEE Trans., Microw. Theory Tech., **6** (2005), 2129–2138.

[9] Montesinos, R.; Berland, C.; Abi-Hussein, M.; Venard, O.; Descamps, P.: Comparative analysis of LINC transmitter performances with class AB and class F power amplifiers, in New IEEE 9th Int. Circuits and Systems Conf. (NEWCAS), 233–236, June 2011.

[10] Colantonio, P.; Giannini, F.; Limiti, E.: High Efficiency RF and Microwave Solid State Power Amplifierss. John Wiley & Sons, 2009.

[11] Cripps, S.C.: RF Power Amplifiers for Wireless Communications. Artech House, Norwood, MA, 2006.

[12] Wright, P.; Lees, J.; Benedikt, J.; Tasker, P.J.; Cripps, S.C.: A methodology for realizing high efficiency class-J in a linear and broadband PA. IEEE Trans. Microw. Theory Tech., **12** (2009), 3196–3204.

[13] Wood, S.; Smith, P.; Pribble, W.; Pengelly, R.; Crescenzi, J.: High efficiency, high linearity GaN HEMT amplifiers for WiMAX applications, 2006, available at: http://www.cree.com/products/wireless_docs.asp

[14] Kazimierczuk, M.K.: RF Power Amplifiers. Wiley, Ohio, 2008.

[15] Grebennikov, A.; Sokal, N.O.: Switchmode RF Power Amplifiers. Newnes, New York, 2007.

[16] Kim, J.H. et al.: Modeling and design methodology of high-efficiency class-F and class-F^{-1} power amplifiers. IEEE Trans. Microw. Theory Tech., **1** (2011), 153–165.

[17] Raab, F.: Class-f power amplifiers with maximally flat waveforms. IEEE Trans. Microw. Theory Tech., **11** (1997), 2007–2012.

[18] Colantonio, P.; Giannini, F; Leuzzi, G.; Limiti, E.: On the class-F power amplifier design. Int. J. RF Microw. Computer-Aided Eng., **9** (1999), 129–149.

[19] Colantonio, P.; Giannini, F; Leuzzi, G.; Limiti, E.: High efficiency low-voltage power amplifier design by second harmonic manipulation. Int. J. RF and Microw. Comput.-Aided Eng., **10** (2000), 19–32.

https://doi.org/10.1017/S1759078711001085 Published online by Cambridge University Press



Ronald Montesinos received the B.Sc. degree in electronic engineering from the National University of Engineering, Lima, Peru, in 2004. He received the B.Eng. degree in microelectronics and telecommunications engineering from Polytechnique School ofMarseille and the M.Sc. degree in wireless devices from University of Provence, Marseille, France, 2009. Since November 2009, he has worked toward his Ph.D. degree in Electronic and Micro-Nano electronic at electronic systems department of ESIEE Paris, Noisy-le-grand, France. His interest areas encompass RF power amplifiers, microwave components and circuts design, and RF transmitter architectures.



Corinne Berland received the B. Eng. degree in electrical engineering from ESIEE Paris, Noisy Le Grand, France, in 1989, and the Ph.D. degree from the University of Marne La Vallée in 2001. From 1989 to 1998, she was with Alcatel Business Systemsand joined ESIEE Paris, in 1998, as an associate professor in the electronic systems department. She is now also with LaMips, Caen, France, for her research activities. Her main interests include transceiver architecture for radiocommunication systems and RF/analog – integrated circuits.



Mazen Abi Hussein received the B.Eng. in electrical engineering from the Lebanese University, Beirut, Lebanon, in 2004, and the M.S. and Ph.D. degrees in electrical engineering from the polytechnique school of Nantes, France, in 2005 and 2009, respectively. From 2006 to 2009, he was with Thales, Cholet, France, as a research engineer, and he is currently a research engineer with ESIEE Paris, Noisy-le-Grand, France. His interests include wireless communications, nonlinear behavioral modeling, linearization techniques for high – power transmitters, and design of 3G transceiver architectures.



Olivier Venard is an associate professor in Signal Processing and Telecommunication in the Telecommunication Department at ESIEE Paris, University Paris-Est since 1997. He conducts his research work in the LaMIPS laboratory. His interests are in the field of signal processing, digital communication, and digital software and hardware architecture.



Philippe Descamps received the Ph.D. degree from the University of Lille, France, in 1992. From 1989 to 1999, he joined the research group Integrated Systems at the Institut d'Electronique, de Microélectronique et de Nanotechnologies (IEMN), Villeneuve d'Ascq, France, where he was involved in microwave research activities mainly guided by the characterization, simulation and design, and by the realization of field-effect devices in centimeters and millimeters wave ranges for automotive applications and telecommunication systems. In 1999, he became a full Professor at the Ecole Nationale Supérieure d'Ingénieurs de Caen (ENSICAEN), France where he currently heads the mixed research Laboratory of Microelectronics and Physics of Semiconductors (LaMIPS). He is mainly involved in high frequencies characterization, modelization of microwave components, and of the design of integrated circuits for telecommunication applications.

https://doi.org/10.1017/S1759078711001085 Published online by Cambridge University Press